TÉCNICO LISBOA

Master's Degree in Electrical and Computer Engineering

Laboratory work

COMPUTER CONTROL

Identification and Computer Control of a Flexible Robot Arm Joint

PART I

Authors: João Prata 69933
Luís Rei 78486
João Girão 78761

November 5, 2017

Contents

List of Tables

List of Figures

Nomenclature

Greek symbols

α	Angle of deflection of the flexible bar with respect to the motor shaft angular direction (in [rad] or [degree])
α_e	Electrical tension in Volts [V] yielded by the sensor of α
ω	Motor angular speed in [degree/s]
ω_e	Electrical tension in Volts [V] yielded by the sensor of ω
θ	Angle of rotation in degrees of the motor shaft with respect to a "zero" direction
θ_e	Electrical tension in Volts [V] yielded by the sensor of θ

Roman symbols

D	Distance of deflection of the bar in meters [m]
K_e	Flexible bar deflection transducer constant in [degree/V]
K_p	Motor shaft angular position transducer constant in [degree/V]
L	Bar length in meters [m]
y	Total angular position in [rad] of the tip of the flexible bar tip with respect to the "zero" direction ($y = \theta + \alpha$).

1 Introduction

The objective of this work consists of the identification and computer control design for the position of a flexible joint of a robot arm - a flexible bar. The work proposed here is in the spirit of Control applied to Cyber-Physical Systems, where a computer is attached to a physical plant (a flexible robot arm joint) to modify its physical behavior through the interaction with the computational part (the computer algorithm).

The work is separated in two parts. In part 1, a plant model that relates the motor that drives the arm with the angular position of its tip is obtained using System Identification methods and data obtained from experiments performed with the plant. In part 2, a controller is designed using the previously obtained model in order to drive position the tip of the robot joint to a desired angle. The controller is then tested on the actual plant.

Throughout the several sections of this report we provide answers to the questions made in the guide, as well as present and comment the experimental results obtained in the first three laboratory sessions.

All the code is made available to allow for the reproduction of the experimental outcomes.

2 Plant description (Question 1)

The plant is a single joint of a flexible robot arm and consists of a DC motor, driven by a power amplifier, whose shaft is united with one extremity of a flexible bar (the joint). Figure 1 below shows a picture of the physical system (the "plant") to control.

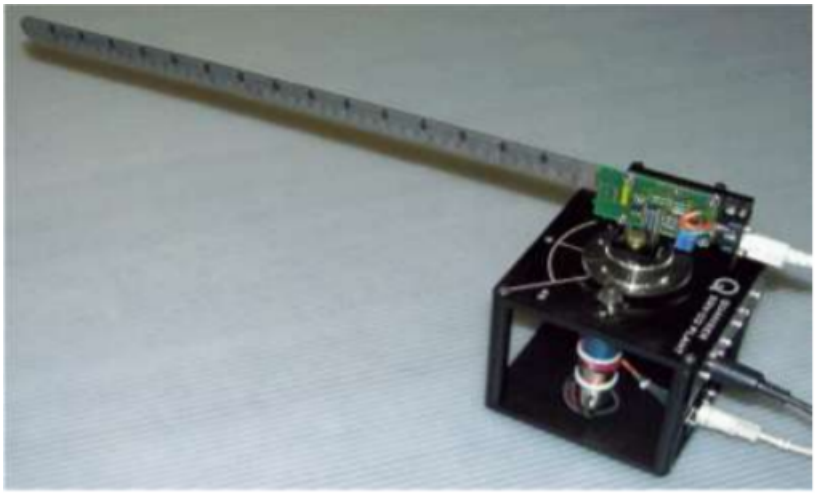

Figure 1: The physical system to control.

The control objective is to actuate on the motor such that the tip of the bar tracks a specified angle. It is not possible to develop a table of electric tensions to apply to the DC motor such that the bar tip moves to a constant position; due to the way the motor's sensor is built there will always be an error between it's angle measurement and the real value. When a constant tension is applied, the angular velocity tends to stabilize, but the shaft always preserves small oscillations and the position of the tip remains with a non-linear behavior. As these oscillations remain throughout time we can assume a plausible rough distribution of two conjugate poles inside the region $|z| < 1$, as well as a real pole and a pole in $z = 1$ due to the motor and the signal integration (velocity/position) it performs. We can also expect a non-minimum phase zero outside the unit circle which causes the system to react with a whiplash like effect right after the beginning of the excitation signal.

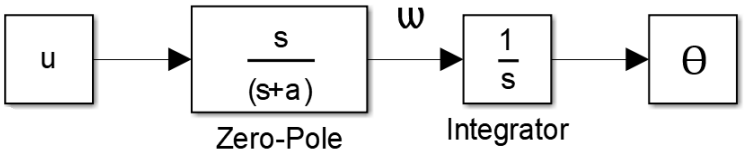

Figure 2: Approximation of the motor's model

The complexity of the problem makes it so that performing feedback on a controller made of a single gain amplifying the tracking error is not enough to solve the issue.

In the next section, the calibration process developed in the first laboratory session will be explained and the outcomes presented.

3 Calibration (Question 2)

The flexible bar is instrumented with a strain gauge, an electrical resistance whose value changes when its length varies. When external forces are applied to a stationary object, stress and strain are the result. Stress is defined as the object's internal resisting forces, and strain is defined as the displacement and deformation that occur. For a uniform distribution of internal resisting forces, stress can be calculated by dividing the force, F, applied by the unit area, A,

$$Stress(\sigma) = \frac{F}{A}.$$

Strain is defined as the amount of deformation per unit length of an object when a load is applied. Strain is calculated by dividing the total deformation of the original length by the original length (L),

$$Strain(\varepsilon) = \frac{\Delta L}{L}.$$

When the bar is deflected, one of its faces is slightly stretched, while the other is compressed; the changes being approximately proportional to the bar tip deflection.

3.1 Measuring the bar deflection

With respect to the circular movement of the motor and the tip of the flexible bar, figure 3, we consider:

- L, the bar length in meters;
- D, the length of the deflection of the bar tip in meters;
- α, the angular deviation of the bar tip with respect to the motor shaft direction in radians;
- θ, the angle of the motor shaft direction with respect to a "zero" direction in radians;

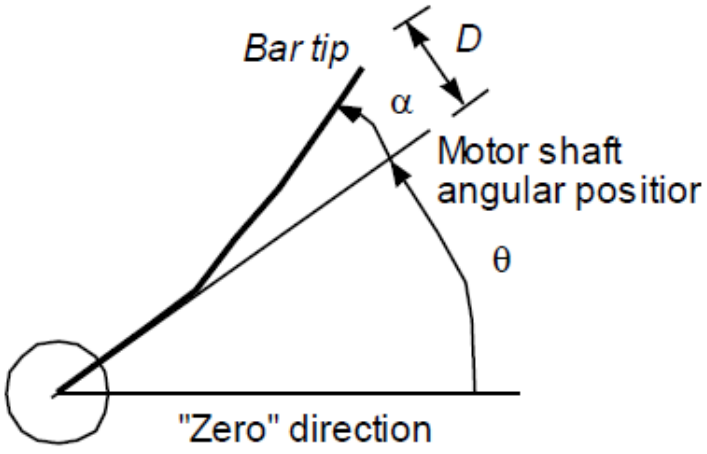

Figure 3: Schematic model of the flexible bar deflection.

Inspecting figure 3 brings us the relation of the angular deflection of the bar tip with its deflection (measured along a straight line),

$$\alpha = \frac{D}{L} \qquad in(rad). \tag{1}$$

From now on, and for the sake of an easier interpretation, the angles presented will be expressed in degrees. The transformation from (1) to the desired unit is done by

$$\alpha_{[degree]} = \frac{180}{\pi} \cdot \alpha_{[rad]}.$$

The total angle that defines the position of the tip of the flexible bar is

$$y = \theta + \alpha. \tag{2}$$

3.2 Flexible bar deflection transducer

The electric tension provided by the angle sensors is but an image of the corresponding angle, as the relation between them is not exactly proportional. This tension α_e is related to the actual deflection of α through

$$\alpha = K_e \alpha_e, \tag{3}$$

where K_e is a constant in [degree/V].

To estimate this constant, a series of experiments are done with the help of a comb with 15 positions (figure 4).

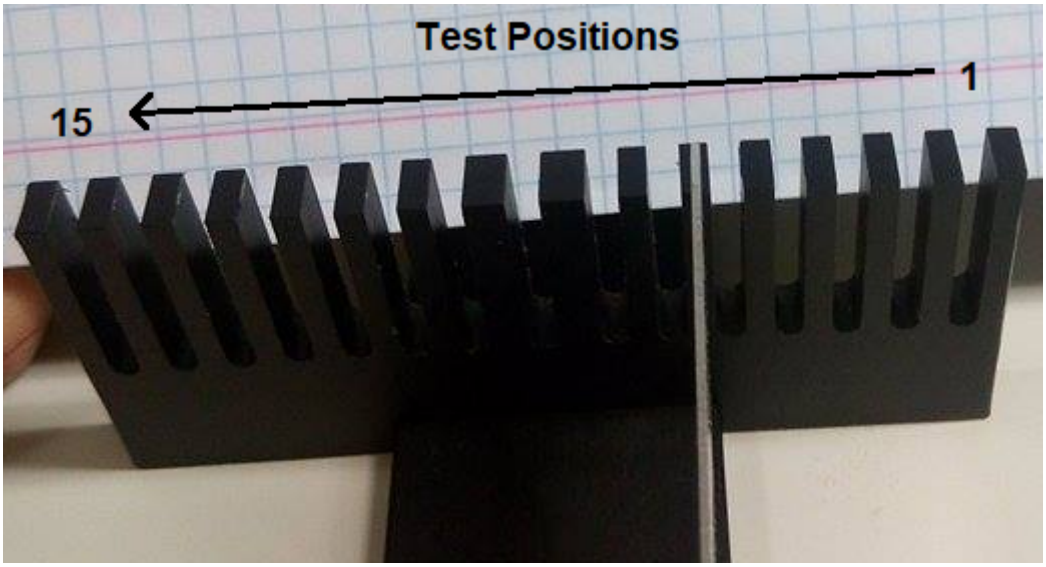

Figure 4: Comb used on the calibration

The bar is deflected by a known quantity, and the tension yielded on the sensor measured using a simulink represented in figure 5. Note that our acquisition board was National Instruments PCI-MIO-16E-4.

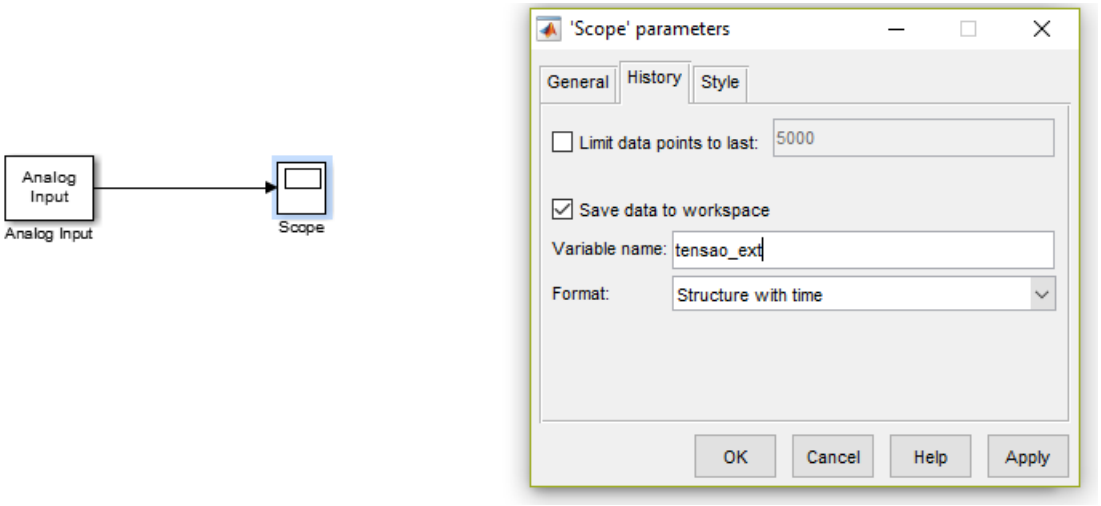

Figure 5: Simulink block diagram used to perform α sensor calibration

Initial configuration has the flexible bar, with a length L of 38.54 [cm], mounted on its calibration rig (illustrated in figure 6) and the output signal visualized through a scope (figure 7).

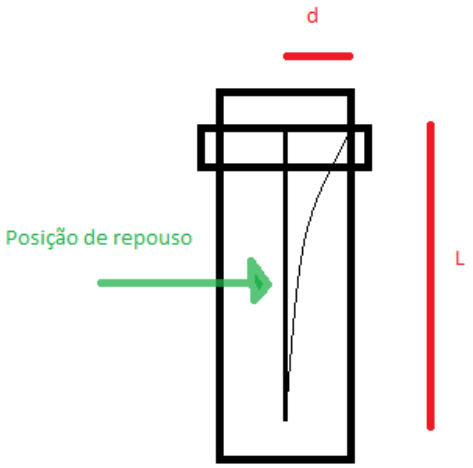

Figure 6: Representation of the calibration "comb" for two different bar deflections: rest position (with no deflection) and deflected to the right most position.

Note that our particular bar (model Quanser 03021) had its rest position slightly to the right, approximately resting between the 5th and 6th comb position.

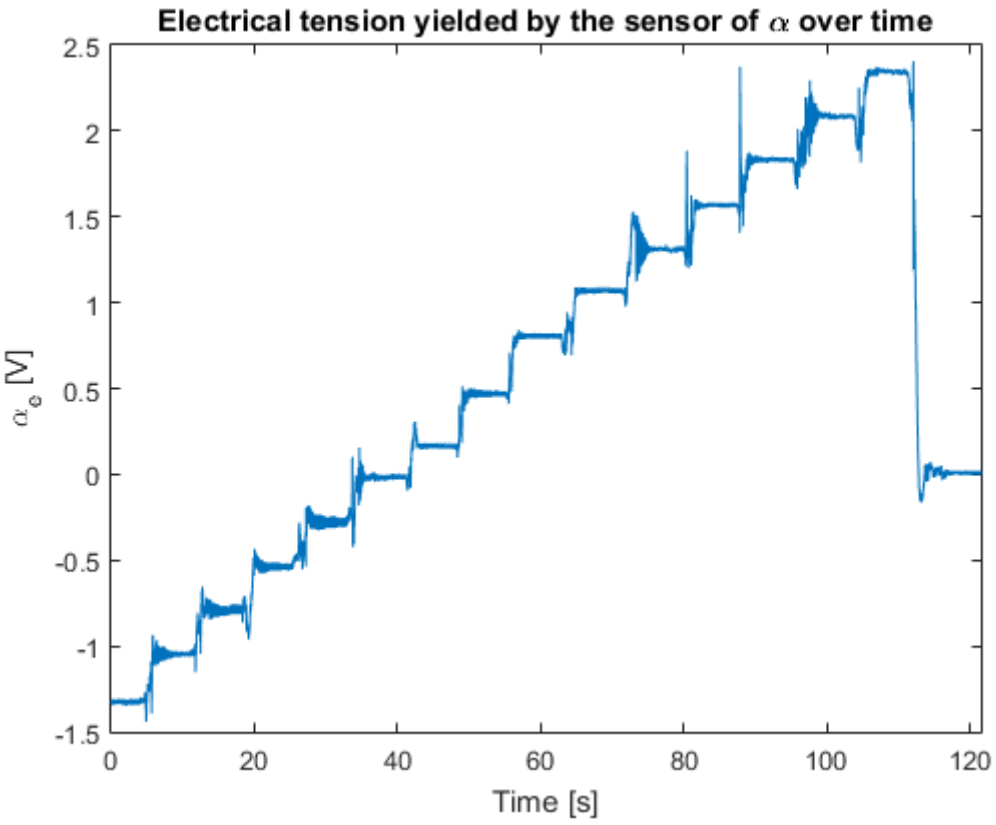

Figure 7: Electrical tension yielded on the transducer on positions of the comb 1 to 15

The α results presented in table 1 were obtained after analysing each section of the previous figure and computing its average.

Table 1: Potentiometer sensor calibration data

Position	d [cm]	α [°]	α_e [V]
1	2.8	4.16	-1.32
2	2.2	3.27	-1.05
3	1.5	2.23	-0.79
4	0.9	1.34	-0.54
5	0.3	0.45	-0.28
6	-0.1	-0.15	-0.02
7	-0.7	-1.04	0.16
8	-1.5	-2.23	0.47
9	-2.3	-3.42	0.81
10	-2.9	-4.30	1.07
11	-3.5	-5.19	1.31
12	-4.2	-6.22	1.57
13	-4.8	-7.10	1.83
14	-5.5	-8.12	2.09
15	-6.1	-9.00	2.34

The small random fluctuations from experiment to experiment and the non-linear relation between the two angles mean that the set of data extracted needs to be treated in order to correspond

K_e to an average behavior (figure 8). Using least squares we estimate K_e = -3.6001 [°/V] as we come up with the best linear correlation in $y = -3.6001x - 0.5186$.

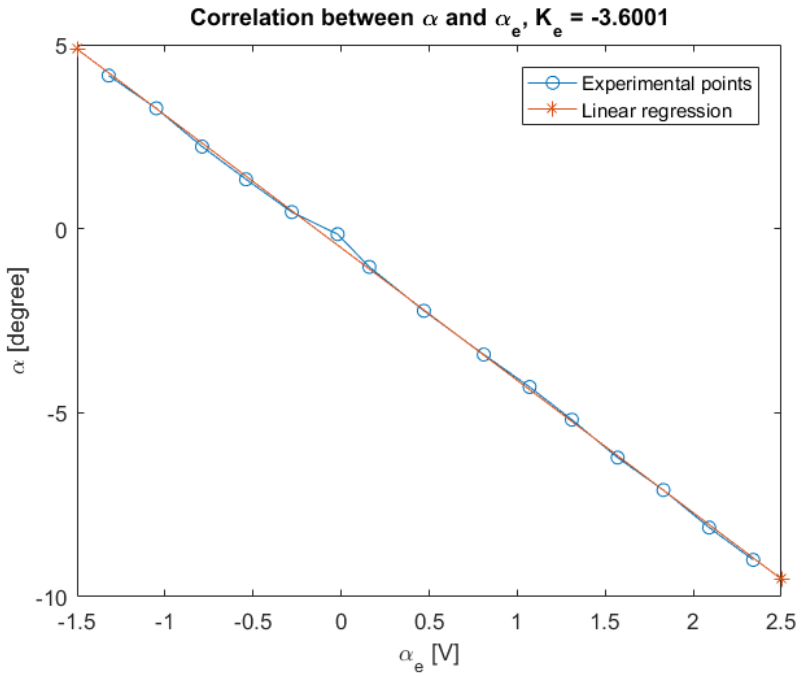

Figure 8: Correlation between α and α_e

3.3 Shaft angle transducer

The shaft angle is measured with a rotation potentiometer whose axis is rigidly connected to it. The potentiometer works by connecting one of the terminals to a resistive strip in form of a coil through a wiper and two other terminals, one at each end of the strip (figure 9). The resistance between one of the end terminals and the middle one is proportional to the angle of the contact. However, because the strip is coiled the device will only produce discrete measurements.

Figure 9: Scheme of the potentiometer used to measure the shaft angle

The shaft angle θ is approximately given as a function of the sensor output θ_e by

$$\theta = K_p \theta_e, \tag{4}$$

where K_p is a constant in [degree/V].

Due to the coiled structure of the resistance there are quantum levels that cause the resistance to vary in a staircase form when the angle varies. This quantization effect brings errors to the measurements and affects the constant determination just as electronic noise produced by electronic devices, noise from the instrumentation devices, or disturbances caused from the cable attached to the shaft do.

To gather the desired θ measurements the simulink block diagram in figure 10 was utilized and, following the guide, a 1 Volt step signal was applied in the motor.

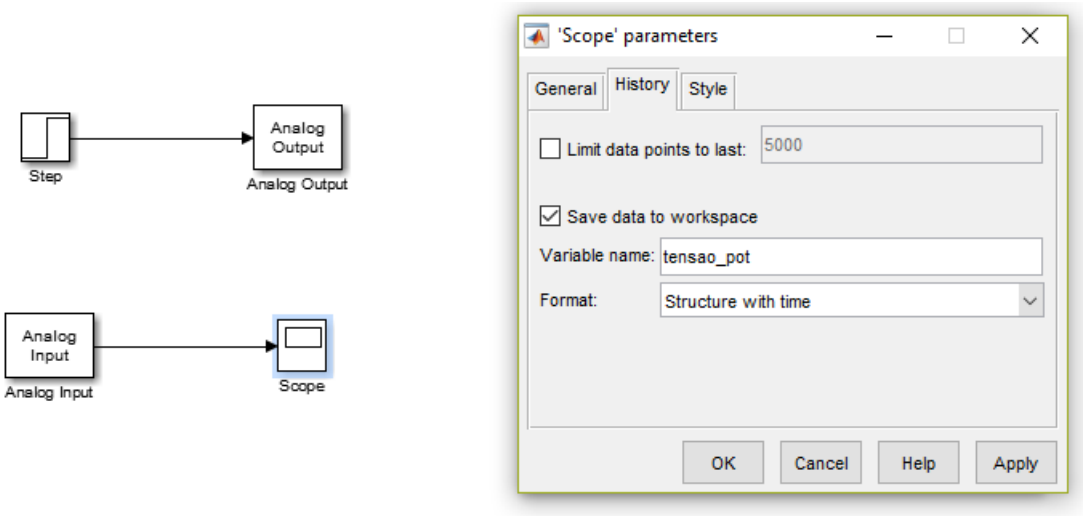

Figure 10: Simulink block diagram used to perform θ sensor calibration

Please notice that applying a positive signal at the entrance makes the motor rotate the arm clockwise, as shown in a video here.

The signal observed in the scope block is presented in figure 11.

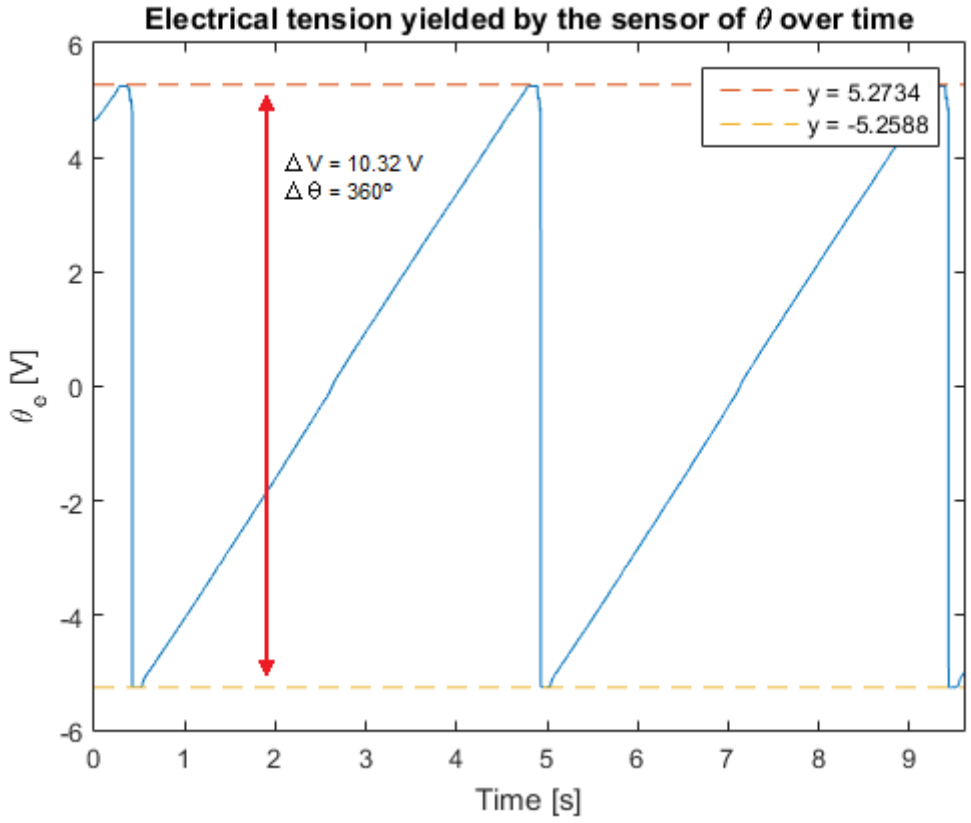

Figure 11: Electrical tension yielded on the potentiometer

Applying a positive tension to the motor implies a positive K_e, K_p. Through analysis of the figure above we obtain

$$K_p = \frac{\Delta\Theta}{\Delta V} \simeq \frac{10.32}{360} = 34.1808[^\circ/V] \tag{5}$$

This result is slightly inferior to the one in the motor's user manual - which was cataloged as being $35.2 \pm 2\%$, making the lowest expected catalog value 34.5 -, but this may be explained by noise on the readings and equipment deterioration.

4 Plant Model Identification (Question 3)

In this section we aim to produce a model (through optimal design of a dynamic system) to be used in control design (second part of the laboratory work). Some aspects regarding this task need to be reinforced. As we dig into this infinite solution problem, with distributed mass all over the shaft, we deal with an infinite number of poles. In this fight between model and control quality, the decision is to attempt to approximate the system using a simpler model, neglecting a very precise representations of the output/model.

Two scripts were built during this phase of the project. One script for model identification: where data processing, ARMAX model identification from plant data, and conversion to state model is performed. This file starts by reading plant data stored in a .mat file and produces as output the matrices that define the state model that become available in the MATLAB Workspace; and another for cross validation: where data stored with a square, PRBS and sawtooth signal are loaded from a .mat file and the modeled wave is ran against the real output to validate the sate-space matrices.

Some aspects to consider when collecting data are the experimental conditions under which our results and consequent analysis are built on. First of all, the excitation signal must not have too low or too high of an amplitude (we used 1 V). If the excitation signal's amplitude is too low, the gearbox backlash prevents the bar from moving, and if it is too high, the motor could be subjected to non-linear effects that distort the signal with respect to linear behavior. Both being detrimental to the identification of the plant model.

Secondly, since the electrical tension applied to the motor isn't symmetrical (figures 12 and 13), the bar will respond at different speeds as the applied tension fluctuates from negative to positive and vice-versa, and it will have a tendency to rotate with a drift to one side.

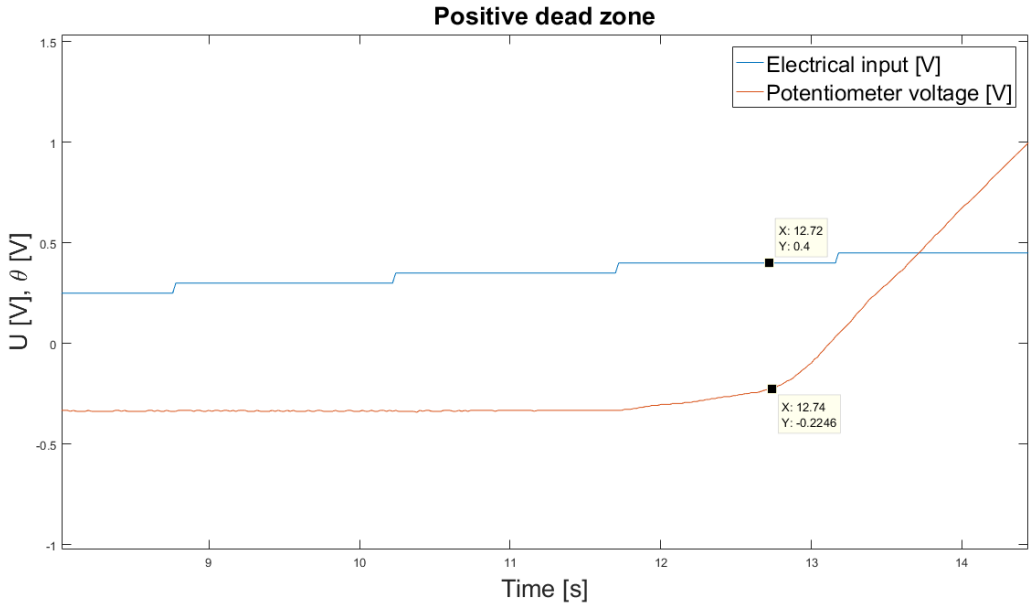

Figure 12: Plant response to a small stepped positive signal

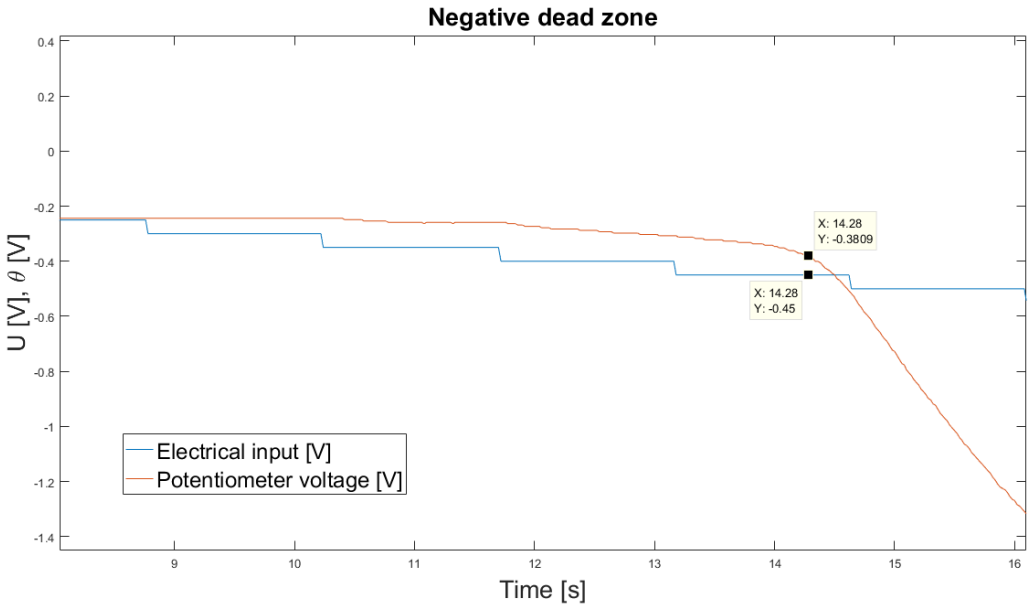

Figure 13: Plant response to a small stepped negative signal

The dead zone thresholds where found by inspection of the ”elbow” curve produced by the plant, with

$$U_{dz}^{+} = 0.4V,$$

and

$$U_{dz}^{-} = -0.35V.$$

To eliminate transient behavior, points corresponding to the first 10 seconds of the data collected were removed and unaccounted for.

Thirdly, we must pay attention to the sampling period (set to 50 Hz) as it has extremely important repercussions on the order of the system to model. For example, modeling a 10 milliseconds delayed signal with a sampling frequency of 10 KHz or 1 KHz is the difference from 1 to 10 samples, the difference between a 1^{st} and a 10^{th} order system. Also, the exciting signal may not be too fast as the plant filters it and is not able to respond in the frequency range where its dynamics is dominant, and may not be too slow since the transients are not excited.

4.1 Experiments

In order to identify the plant model tests with different types of excitation signals were performed, and their response analyzed. The training set for this task consists, firstly, of a square wave with $f = 0.5$ Hz was used. Then, a PRBS - **P**seudo-**R**andom **B**inary **S**equence -, in order to "stress" the plant and get a better scope of how it responds to a random signal. They are presented in figures 14 and 15 respectively.

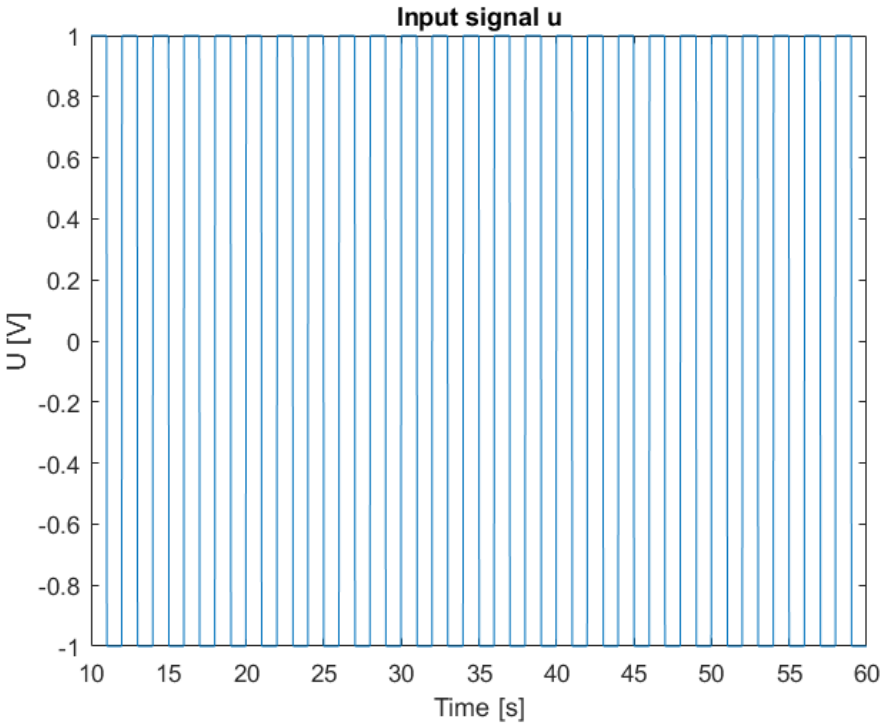

Figure 14: Square wave signal used to excite the motor

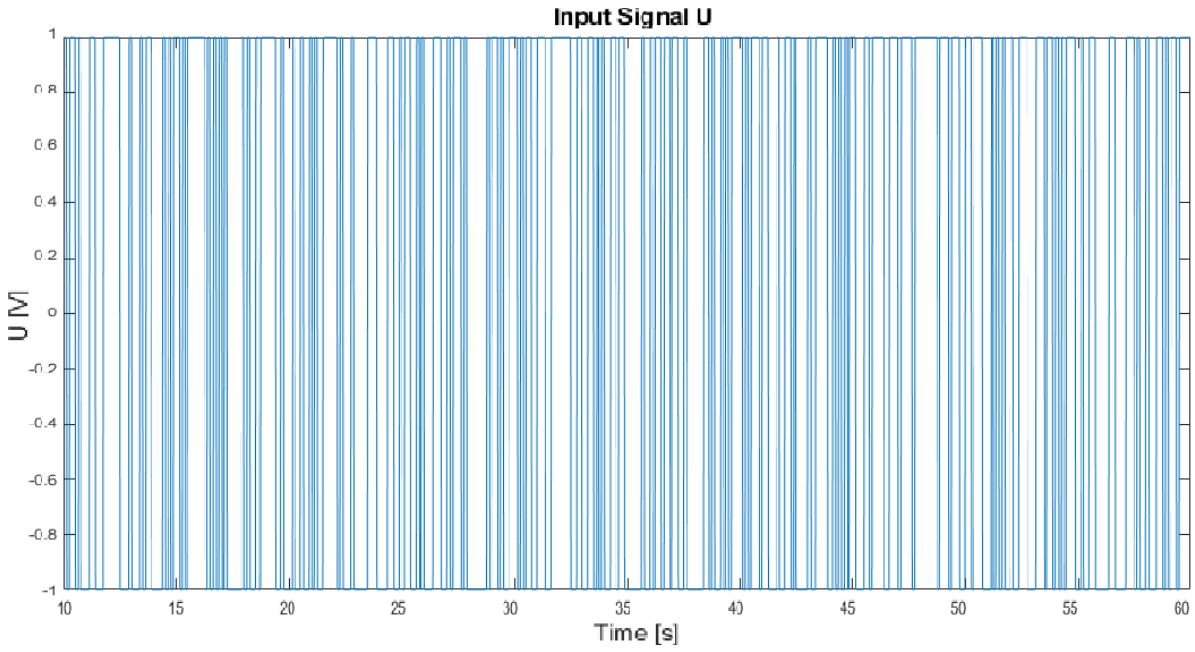

Figure 15: PRBS signal used to excite the motor

After building the data structures and saving the sensor measurements the bar tip angle was reconstructed with the constants calculated in section 3 with

$$y_{trend} = \theta_e \cdot K_p + \alpha_e \cdot K_e, \tag{6}$$

The obtained responses are as follows:

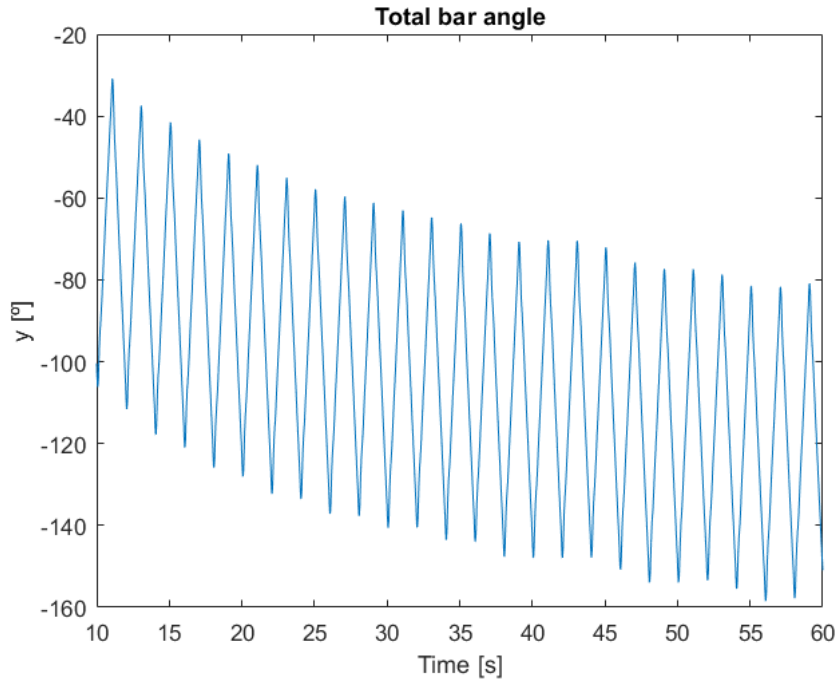

Figure 16: Plant response to square wave excitation signal

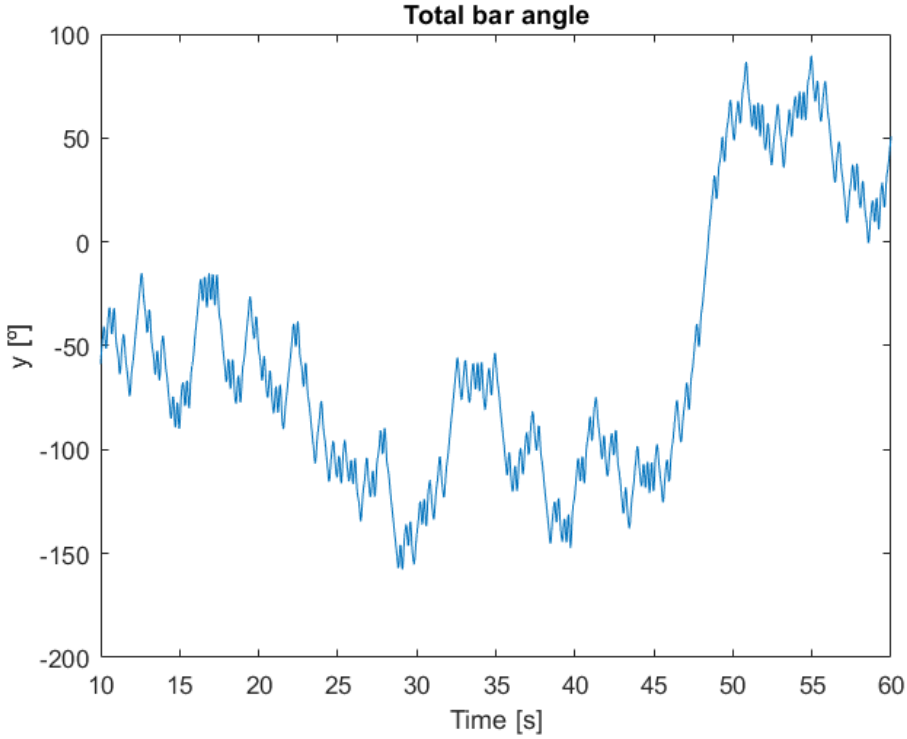

Figure 17: Plant response to the PRBS excitation signal

When using the square wave as excitation signal, there is a remarkable ”drift” as the motor shaft angle steadily grows in time due to the electrical tension applied to the motor not being exactly symmetrical, the input tension signal not having a non-zero average value. We also had to be careful when using the PRBS signal as excitation, because it could easily make the bar do a full spin, making a huge variation in the theta signal, which meant the identification would be worse, since we are going to be using a differentiated response.

To remove the integral effect introduced by the motor given by the relation between the angular speed and the angular position of the motor shaft, a differentiation on the motor shaft angle is performed. Figure 18 shows spectrum of the differentiator block.

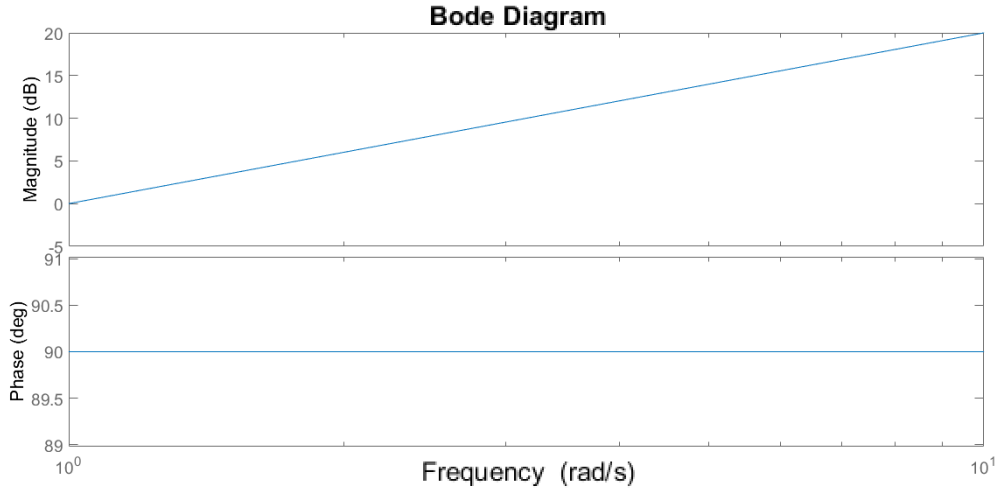

Figure 18: Frequency response to differentiator block.

Directly differentiating the signal sees the noise effect increase quadratically with a frequency gain, and we cannot afford to do this as we'd be swamping the output with noise.

As the noise presents itself by introducing lots of small variations (derivative is of high value), a low-pass filter is used to remove high frequency of noise and render the data usable by stopping the propagation of errors after differentiating.

Tests varying the filter pole confirmed that a small value of 0.5 corresponded to a faster system and that as the filter pole went closer to 1, the lower frequency will start to be cut off sooner, eventually tending to 0 - too much information is lost by filtering to much data. A value of 0.9 proved to be ideal for our purposes.

After removing the average value of the input/output signal, model identification for the signal is performed using the function **armax** of Control Systems Toolbox in MATLAB. Several different orders were attempted to obtain a model with an order that is not to big, but that leads to a good fitting. What will categorize the matrix approximation as good or bad will be the performance of the controller you will design with the model in a later stage of the project.

The **armax** function estimates armax polynomial model using time domain data represented by

$$A(q)y(t) = B(q)u(t-nk) + C(q)e(t), \tag{7}$$

and receives [na, nb, nc, nk] where na, nb, nc and nk are the polynomial orders associated with the armax model,

$$na = order\ of\ A\ polynomial\ (N_y - by - N_y\ matrix) \tag{8}$$
$$nb = order\ of\ B\ polynomial + 1\ (N_y - by - N_u\ matrix) \tag{9}$$
$$nc = order\ of\ C\ polynomial\ (N_y - by - 1\ matrix) \tag{10}$$
$$nk = input\ delay\ (in\ number\ of\ samples,\ N_y - by - N_u\ entries), \tag{11}$$

N_u = number of inputs and N_y = number of outputs, parameter *nk* represents pure delay, an invisible branch contaminated by white noise that passes through the transfer function.

The function has a metric to determine better fit to data, allowing for the measurement of the goodness of the fit and a determination of the model output match on the input. Table 2 summarizes the attempted parameters.

Table 2: Armax model tested parameters

#	na	nb	nc	nk
1	3	2	3	1
2	4	2	3	1
3	4	2	4	1
4	4	3	4	1
5	8	8	8	1

Please note that $nc > na$ was not attempted as it increased the system's memory.

The subtle behavior of the bar is key to make a stable controller, and the most important dynamic behavior of bar is the whiplash - inertia will make the tip move in the opposite direction of the desired one. Through the analysis of the filtered response a notion regarding the quality of the model is gained. Figures 19 to 24 represent alternately responses to the square and PRBS signals of the filtered signal and of the bar angles.

We chose to present graphs only for the first model mainly because the model responses are all graphically similar and also to keep this report concise, with no loss of information.

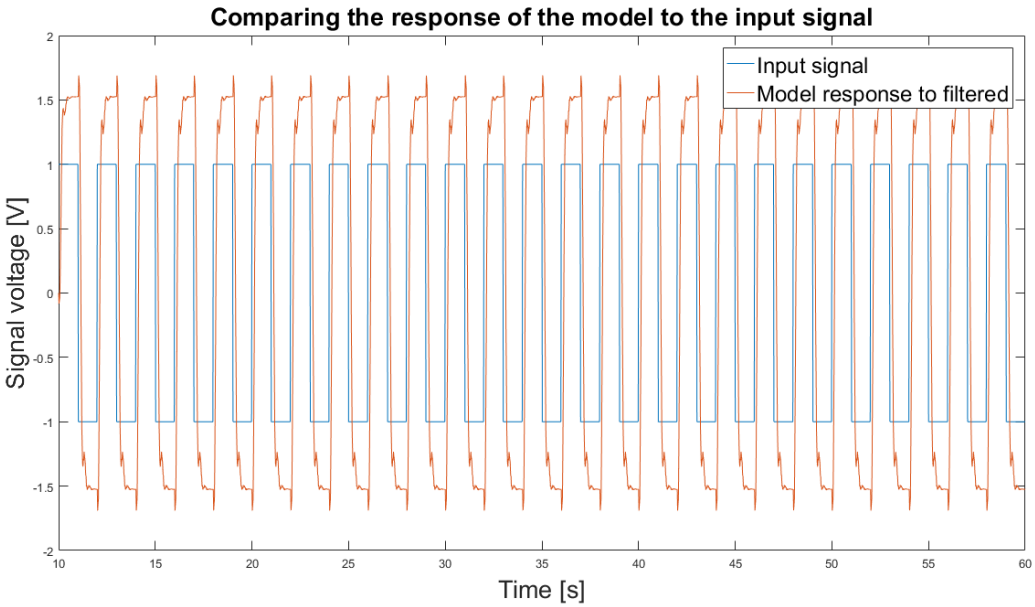

Figure 19: Filtered signal response to square wave input

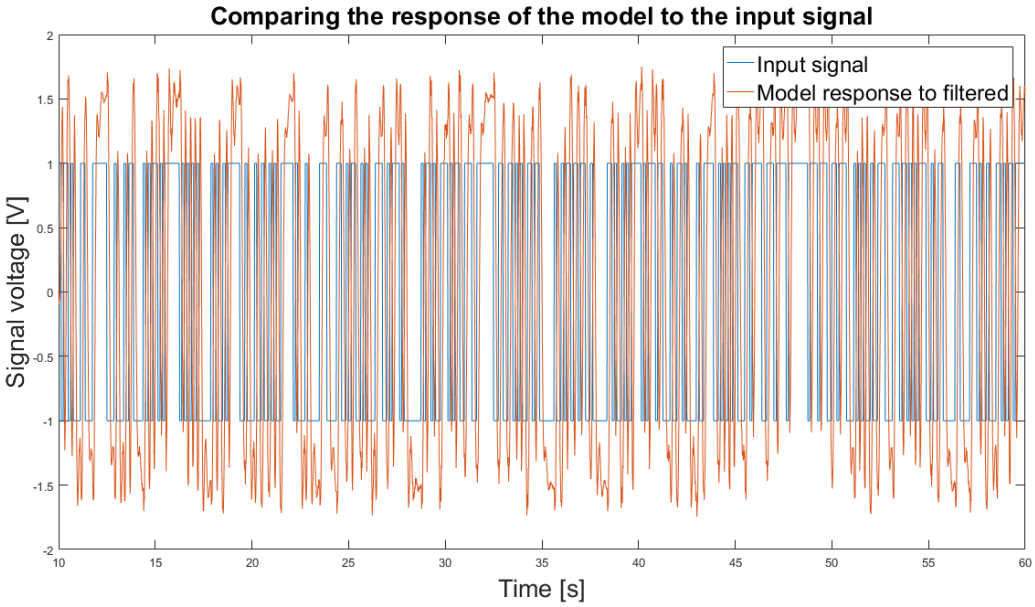

Figure 20: Filtered signal response to PRBS wave input

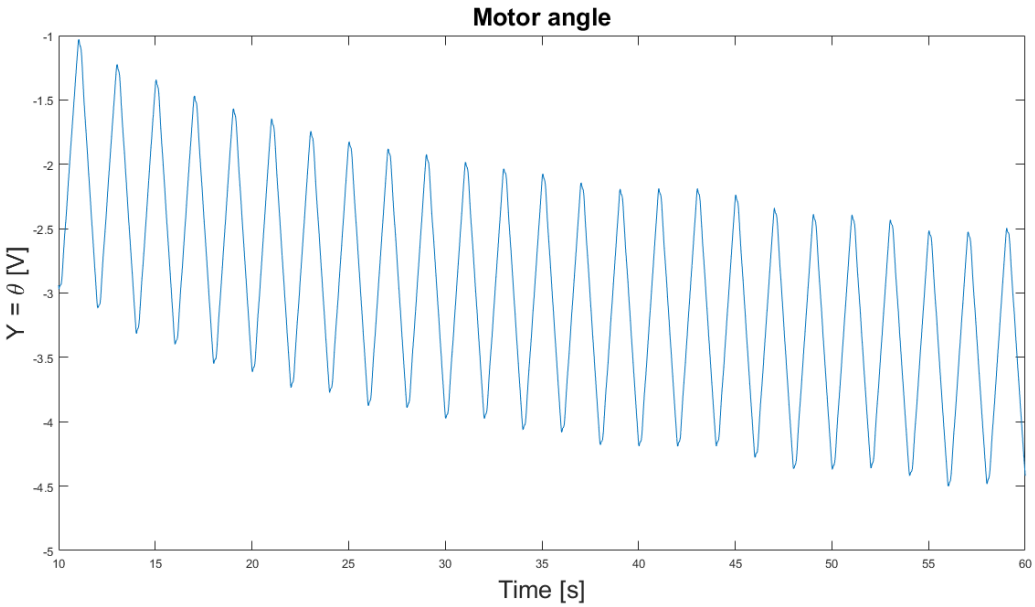

Figure 21: Angle of the motor with square wave input

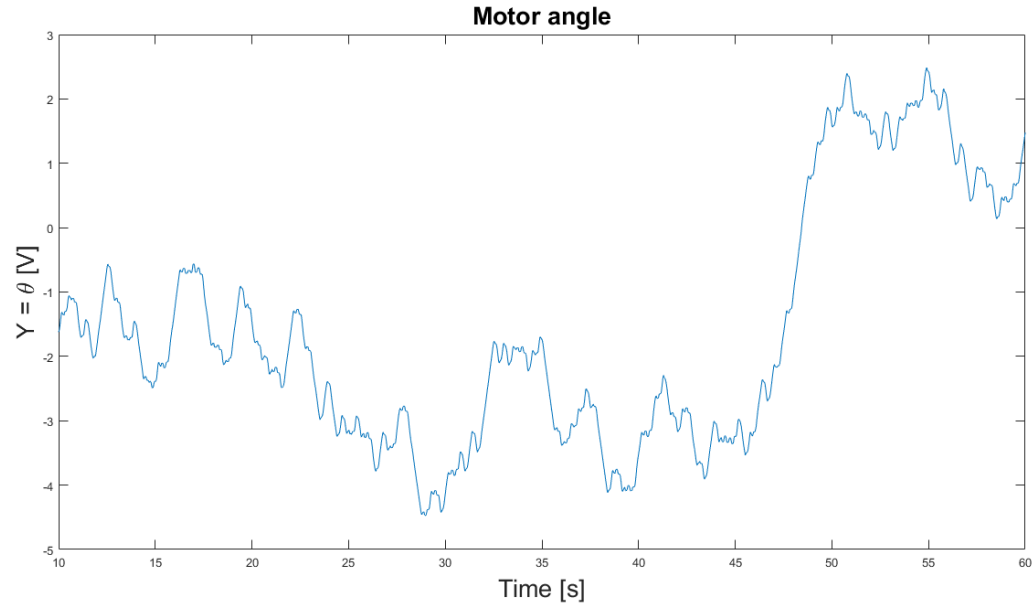

Figure 22: Angle of the motor with PRBS wave input

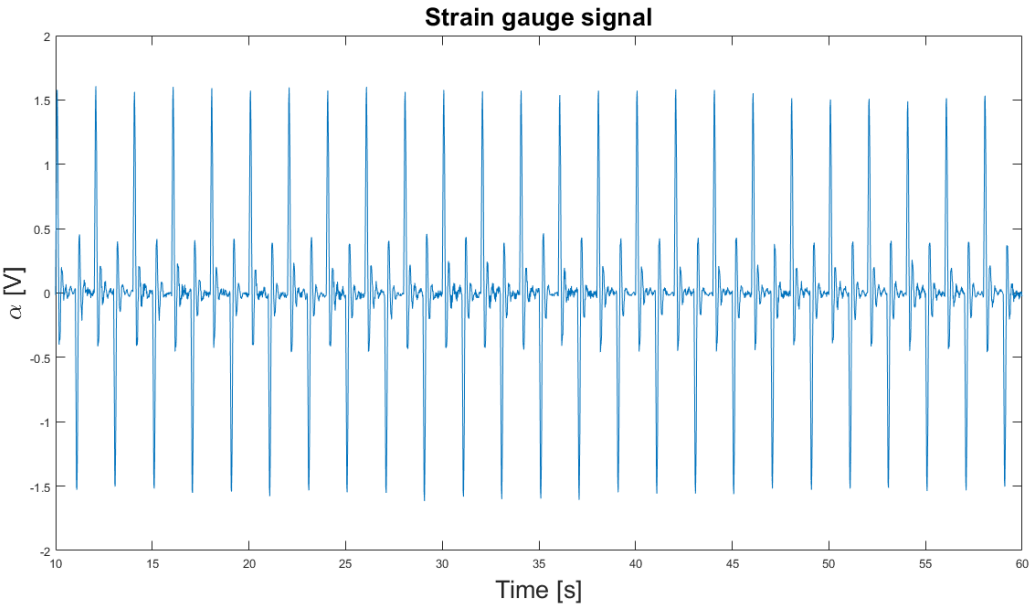

Figure 23: Deflection of the bar tip with square wave input

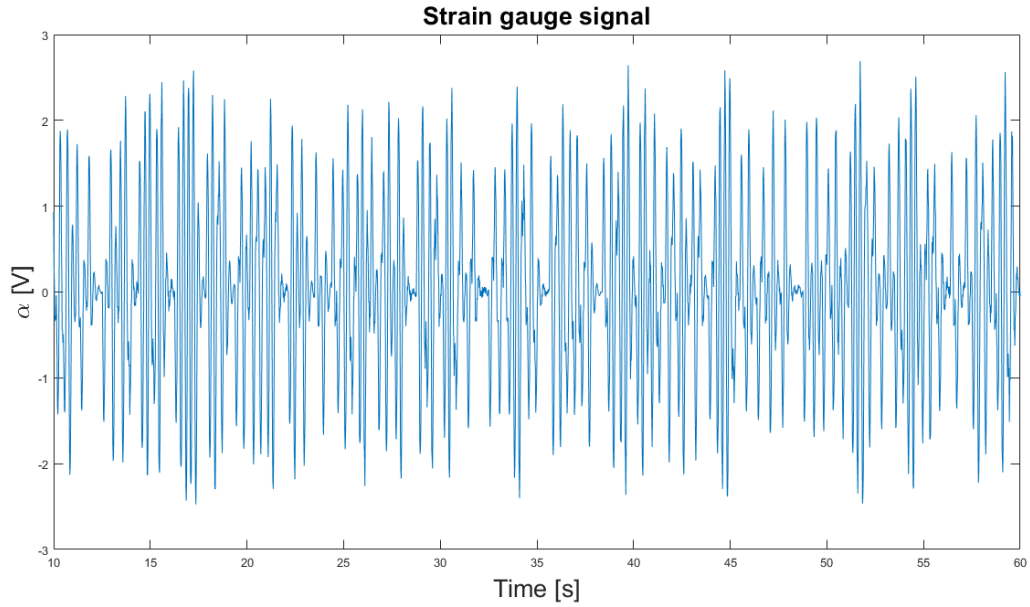

Figure 24: Deflection of the bar tip with PRBS wave input

To characterize the plant open loop a pole-zero plot of all the testes parameters minus the second one is presented in figure 25 and 26. In here, non-minimum phase zeros (outside circle) signals for whiplash behavior. Notice that a bigger order in the denominator than in the numerator translates in a zero at the origin.

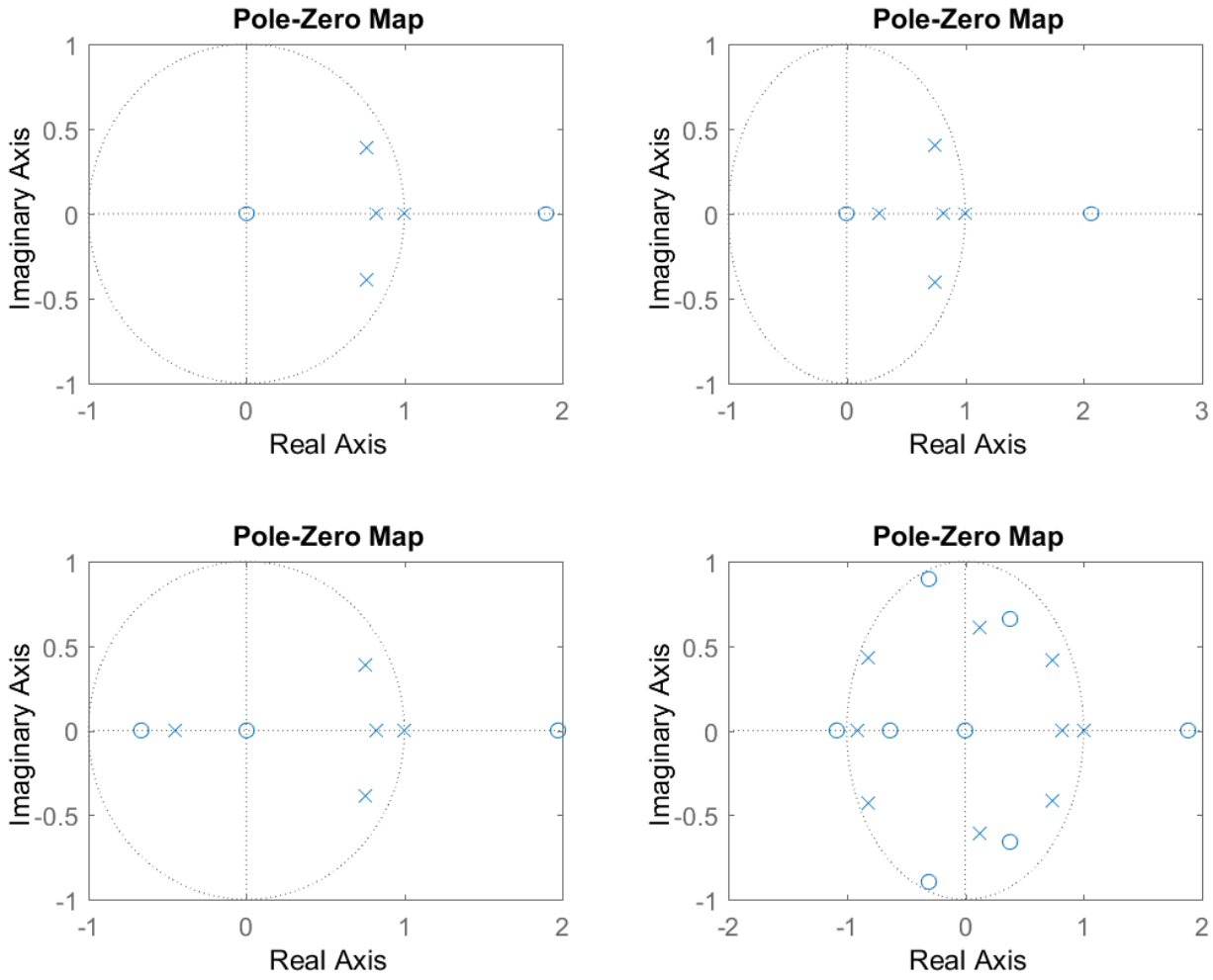

Figure 25: Pole-Zero map of the best models made from the square wave. From left to right, up to down we have: 3-2-3-1 model, 4-2-4-1 model, 4-3-4-1 model and 8-8-8-1 model

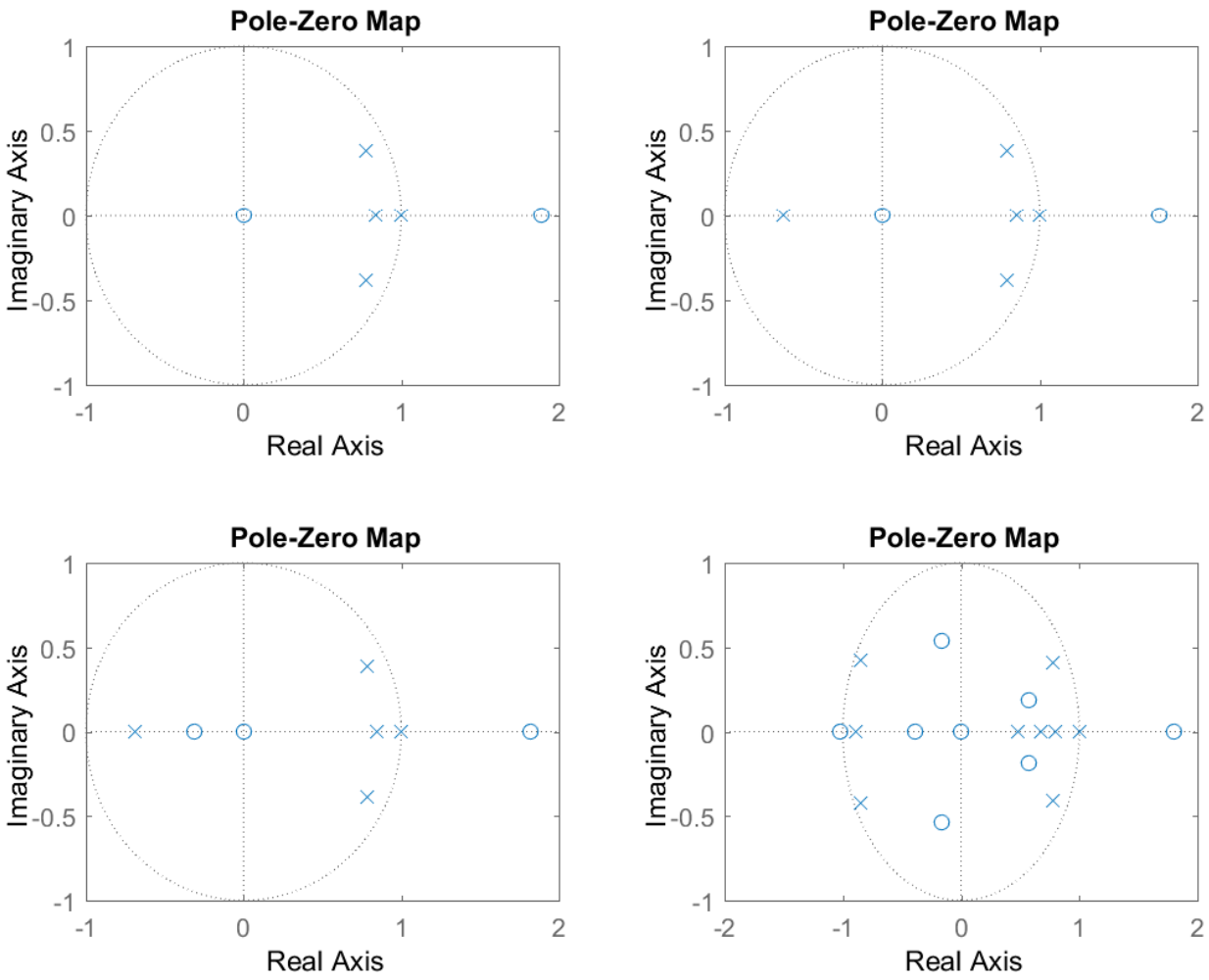

Figure 26: Pole-Zero map of the best models made from the PRBS wave. From left to right, up to down we have: 3-2-3-1 model, 4-2-4-1 model, 4-3-4-1 model and 8-8-8-1 model

4.2 Cross validation

To validate the computed models in section 4.1 a testing set is introduced in the form of a sawtooth signal (figures 27 and 28).

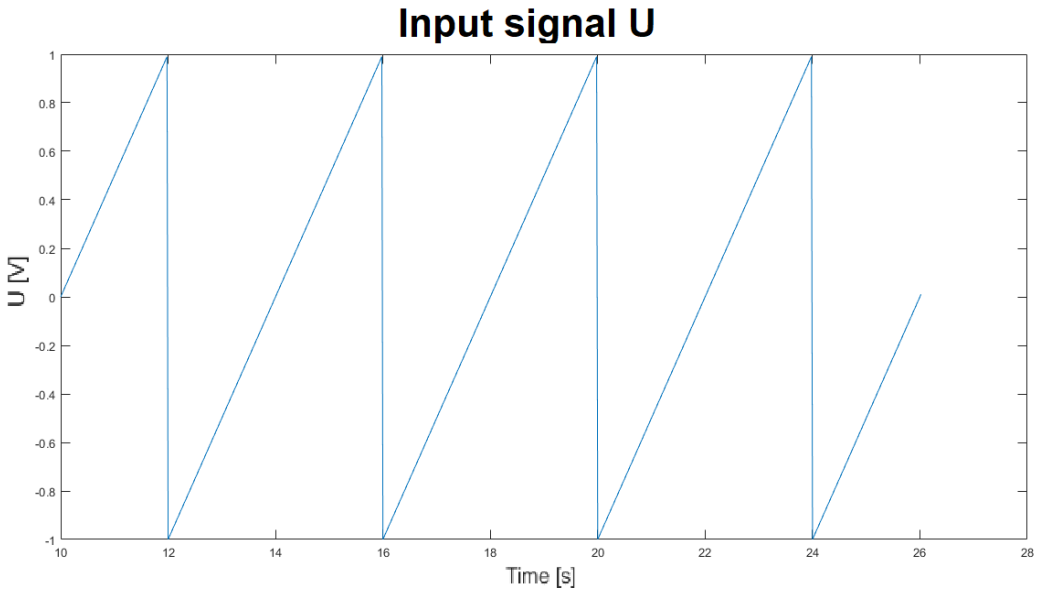

Figure 27: Sawtooth input signal.

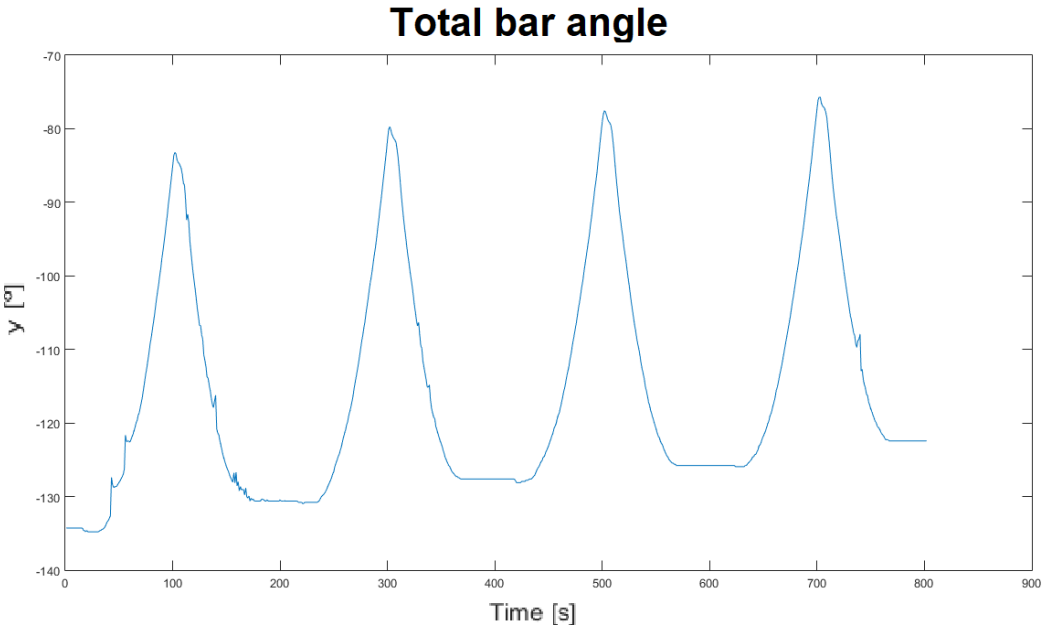

Figure 28: Plant response to sawtooth signal.

To evaluate our parameters and choose the best one to our problem, we performed Cross Validation. To do this, we used the **R**oot **M**ean **S**quared **E**rror metric, which is commonly used to measure accuracy for continuous variables.

$$RMSE = \sqrt[2]{\frac{1}{n}\sum_{j=1}^{N}(y_j - \hat{y_j})^2}$$

Since the errors are squared before they are averaged, the **RMSE** gives a relatively high weight to large errors. This means this metric should be useful when large errors are particularly undesirable as is the case for the problem at hand.

Now, using the various models and performing a simulation with inputs, square wave, PRBS wave and sawtooth wave, the following table was created. As we see in table 3 the root mean squared error is similar to every model.

Table 3: Model analysis

Armax Model	Input signal	Modeling fit [%]	RMSE w/ square input	RMSE w/ PRBS input	RMSE w/ sawtooth input
3-2-3-1	Square	97.19	42.9169*	28.3513	10.3682
4-2-3-1	Square	97.22	43.0658*	28.4387	10.4693
4-2-4-1	Square	97.41	43.0853*	28.4488	10.4853
4-3-4-1	Square	97.43	42.9772*	28.3854	10.4053
8-8-8-1	Square	98.10	42.9430*	28.3717	10.3997
3-2-3-1	PRBS	92.83	43.1880	28.5393*	10.5500
4-2-3-1	PRBS	93.82	43.4642	28.7228*	10.7200
4-2-4-1	PRBS	93.96	43.6404	28.8355*	10.8368
4-3-4-1	PRBS	94.13	43.3910	28.6711*	10.6760
8-8-8-1	PRBS	96.11	42.7850	28.3063*	10.2975

*should not be considered for cross-validation purposes, only there for comparison.

The more complex model, with 8 poles and 8 zeros, corresponding to the yellow rows, is the best overall in the cross-validation tests, approximating it the closest to the real signals. However, this makes it so that it's much harder to project a good controller for the plant later on. The final ARMAX model is represented by the first set of parameters from table 2 - 3 poles and 2 zeros. The simpler model, represented in green rows, comes as the second best in the cross-validation tests and represents a much simpler to design our control around in the second part of the laboratory work.

It should be noted that the difference in error is negligible, making our go-to choice of the simpler model that much intuitive.

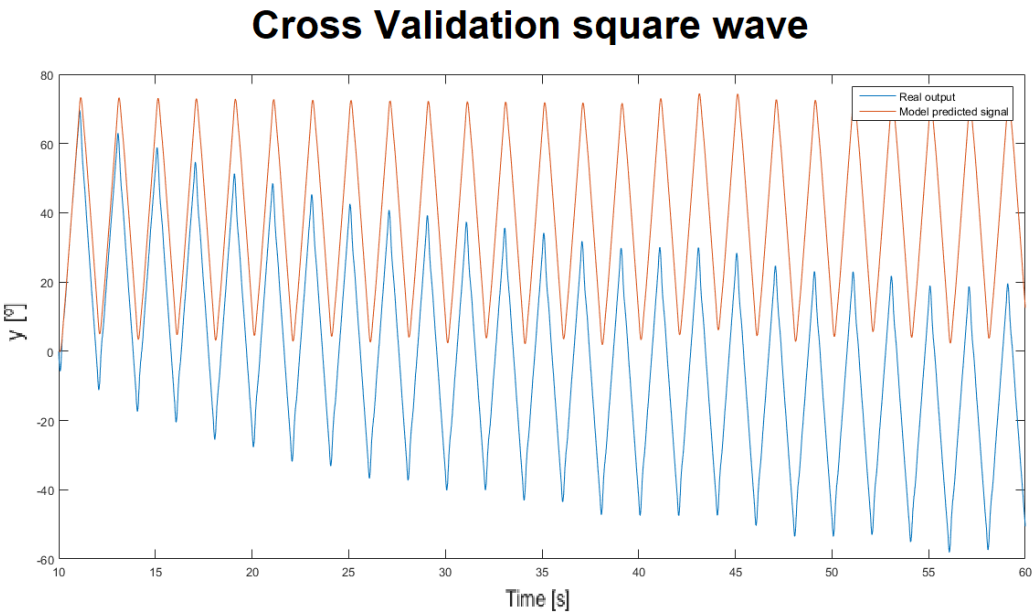

Figure 29: Cross Validation between Plant response and Model response to a square wave

The difference between the modeled output signal and the real one is due to the mean being non-zero. From an analysis point of view this is irrelevant but to visually improve the result when presented the mean of the signal is subtracted.

Against our testing set the best model was damaged by the dead zone as its behavior is unpredicted. That way the non-linearity is not followed.

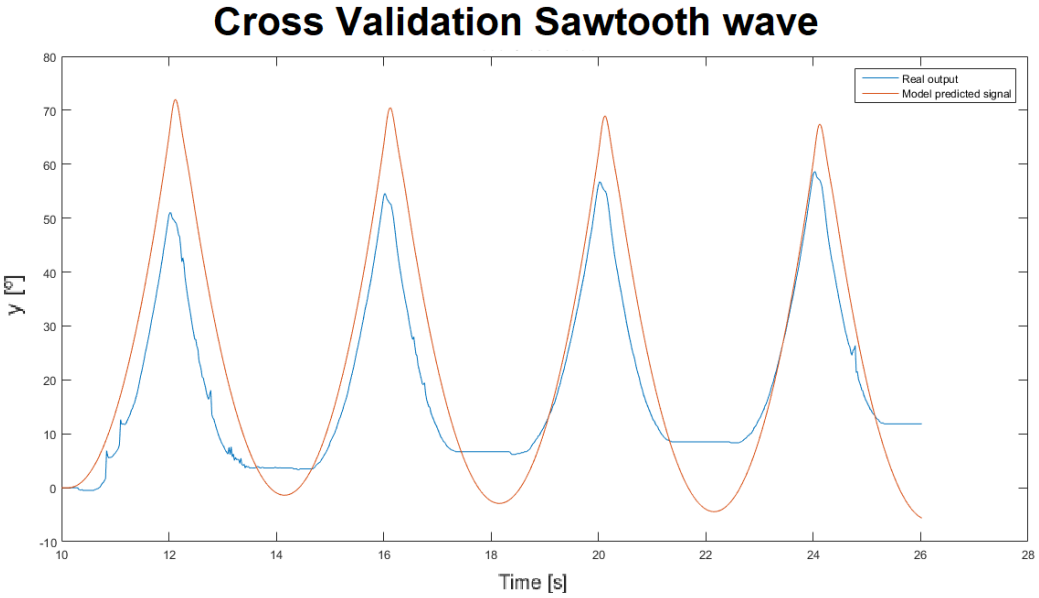

Figure 30: Cross Validation between Plant response and Model response to a sawtooth wave

We make a clear equivalence between the model's frequency response and the pole-zero mapping.

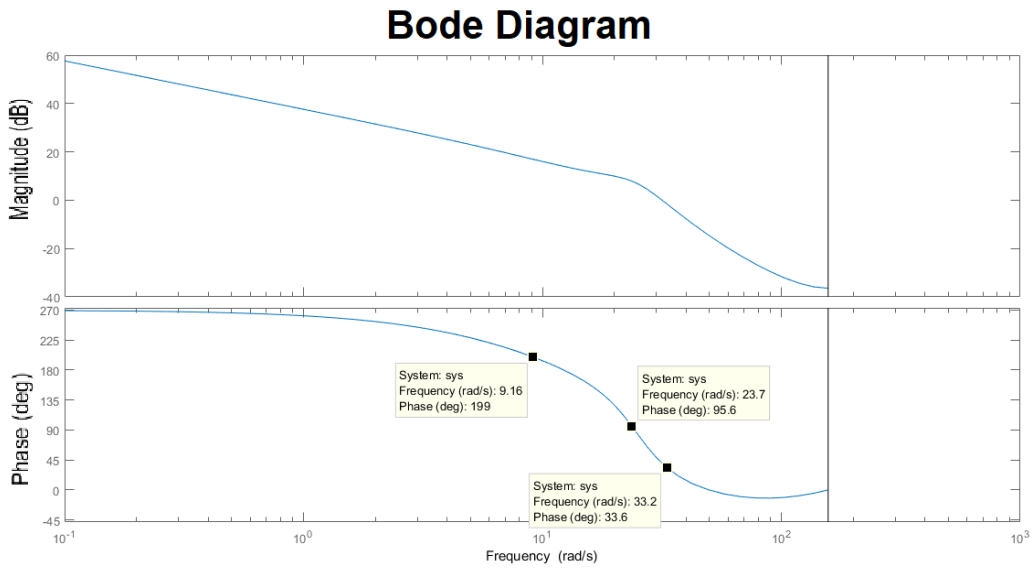

Figure 31: Frequency Response of the chosen model

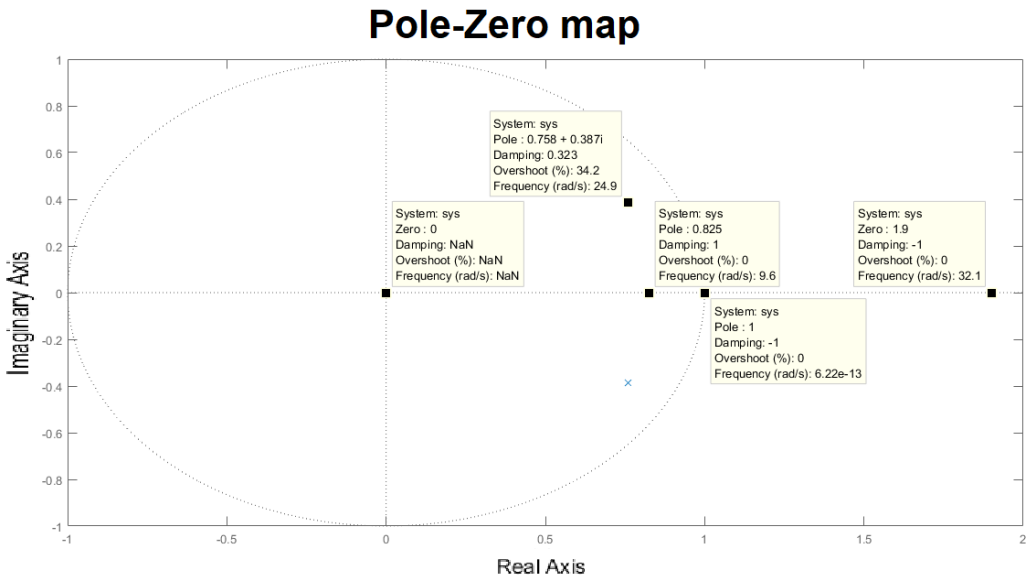

Figure 32: Pole-Zero map of the chosen model

The final state-space model is described as

$$A = \begin{bmatrix} 3.3417 & -4.3177 & 2.5739 & -0.5979 \\ 1.0000 & 0 & 0 & 0 \\ 0 & 1.0000 & 0 & 0 \\ 0 & 0 & 1.0000 & 0 \end{bmatrix},$$

$$B = \begin{bmatrix} 1 \\ 0 \\ 0 \\ 0 \end{bmatrix},$$

$$C = \begin{bmatrix} -0.0615 & 0.1169 & 0 & 0 \end{bmatrix},$$

$$D = 0.$$

These matrices form the input to the next phase of the project, concerned with controller design.